Translational Oncology 49 (2024) 102087

Contents lists available at ScienceDirect

Translational Oncology

journal homepage: www.elsevier.com/locate/tranon

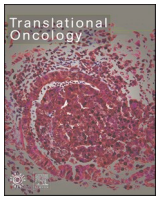

The value of T1- and FST2-Weighted-based radiomics nomogram in differentiating pleomorphic adenoma and Warthin tumor

Hongbiao Sun [a,1], Zuoheng Sun [b,c,1], Wenwen Wang [d,1], Xudong Cha [b], Qinling Jiang [a], Xiang Wang [a], Qingchu Li [a], Shiyuan Liu [a], Huanhai Liu [b], Qi Chen [a,e,2], Weimin Yuan [a,f,2], Yi Xiao [a,2,*]

[a] Department of Radiology, Changzheng Hospital, Navy Medical University, Shanghai, China
[b] Department of Otolaryngology, Changzheng Hospital, Navy Medical University, Shanghai, China
[c] Department of Otolaryngology, Naval Specialty Medical Center, Naval Medical University, Shanghai, China
[d] Department of Neurology, Changzheng Hospital, Navy Medical University, Shanghai, China
[e] Department of Radiology, Kunshan Third People's Hospital, Kunshan, Jiangsu, China
[f] Department of Radiology, Qingdao Special Servicemen Recuperation Center of PLA Navy, Qingdao, China

ARTICLE INFO

Keywords:
MRI
Nomogram
Parotid gland
Pleomorphic adenoma
Warthin tumor
Radiomics

ABSTRACT

Purpose: To establish a radiomics nomogram based on MRI radiomics features combined with clinical characteristics for distinguishing pleomorphic adenoma (PA) from warthin tumor (WT).
Methods: 294 patients with PA (n = 159) and WT (n = 135) confirmed by histopathology were included in this study between July 2017 and June 2023. Clinical factors including clinical data and MRI features were analyzed to establish clinical model. 10 MRI radiomics features were extracted and selected from T1WI and FS-T2WI, used to establish radiomics model and calculate radiomics scores (Rad-scores). Clinical factors and Rad-scores were combined to serve as crucial parameters for combined model. Through Receiver operator characteristics (ROC) curve and decision curve analysis (DCA), the discriminative values of the three models were qualified and compared, the best-performing combined model was visualized in the form of a radiomics nomogram.
Results: The combined model demonstrated excellent discriminative performance for PA and WT in the training set (AUC=0.998) and testing set (AUC=0.993) and performed better compared with the clinical model and radiomics model in the training set (AUC=0.996, 0.952) and testing model (AUC=0.954, 0.849). The DCA showed that the combined model provided more overall clinical usefulness in distinguishing parotid PA from WT than another two models.
Conclusion: An analytical radiomics nomogram based on MRI radiomics features, incorporating clinical factors, can effectively distinguish between PA and WT.

Introduction

Salivary gland tumors are a relatively rare type of head and neck tumors, accounting for about 3–6 % of cases [1]. Approximately 80 % of salivary gland tumors are parotid gland tumors, and roughly 80 % of parotid gland tumors are benign, with pleomorphic adenoma (PA) and warthin tumor (WT) being the two major benign pathological types [2,3]. Although both benign tumors, PA has a higher rate of malignant transformation and recurrence [4], while WT is not cancerous due to slow progression, leading to different treatment methods [5,6]. Therefore, it is particularly important to evaluate parotid tumors by collecting clinical and image information before surgery to make the best

Abbreviation: PA, pleomorphic adenoma; WT, Warthin tumor; ROIS, regions of interests; T1WI, T1 weighted image; FS-T2WI, fat saturation T2 weighted imaging; ICC, inter- and intra- class correlation; LASSO, least absolute shrinkage and selection operator; Rad-Score, radiomics score; ROC, receiver operating characteristic; AUC, area under the curve; DCA, decision curve analysis.

* Corresponding author at: Department of Radiology, Changzheng Hospital, Navy Medical University, No.415 Fengyang Road, Huangpu District, Shanghai, 200003, China.
E-mail address: czyyxiaoyi@163.com (Y. Xiao).
[1] Hongbiao Sun, Zuoheng Sun and Wenwen Wang contributed equally.
[2] Qi Chen, Weimin Yuan and Yi Xiao contributed equally.

https://doi.org/10.1016/j.tranon.2024.102087
Received 22 April 2024; Received in revised form 23 July 2024; Accepted 11 August 2024

Table 1
Clinical factors and MRI features of the training and testing set.

Clinical factors	Training set (n = 205)			Testing set (n = 89)		
	PA(n = 113)	WT(n = 92)	P-value	PA(n = 46)	WT(n = 43)	P-value
Sex (male/female)	55/58	88/4	<0.001	26/20	40/3	<0.001
Age	44.6 ± 15.5	61.4 ± 7.5	<0.001	47.0 ± 14.0	62.7 ± 7.4	<0.001
Smoking: pack-years	2.9 ± 7.6	29.8 ± 16.7	<0.001	5.3 ± 12.5	29.3 ± 17.2	<0.001
Shape (round/not round)	79/34	67/25	0.761	30/16	31/12	0.639
Amount of tumor (single/multiple)	110/3	50/42	<0.001	46/0	22/21	<0.001
Margin (well defined/ill defined)	113/0	89/3	0.177	46/0	40/3	0.217

PA: pleomorphic adenoma, WT: warthin tumor.

treatment plan and surgical method [7,8].

Fine needle aspiration biopsy is a simple and rapid examination method, and previous studies have found that it has a certain value in the diagnosis of benign tumors [9]. However, it is often limited by the scope of the tumor and the level of clinical experience of the operator, which may have the risk of tumor spread and facial nerve injury [10,11].

The accuracy of CT [12] and MRI [13] is 84.7 % and 91.3 % in distinguishing WT from PA, which are important means for preoperative auxiliary diagnosis. But distinguishing between WT and PA based on traditional CT and MR Imaging may be challenging, for the reason that the imaging characteristics of the two tumors are usually very similar [7,14,15]. Therefore, better methods are needed to improve the ability to differentiate PA from WT.

In recent years, radiomics is a new technology that can further improve the means of imaging differentiation and is widely used in oncology. By extracting a large amount of feature information from standard medical images, automatic sequence algorithm can be used to make a more comprehensive description of tumors, showing a better prospect in tumor identification, treatment effect evaluation and prognosis prediction [16-18]. With the development of artificial intelligence and the increase of algorithms, the accuracy of preoperative diagnosis can be better improved through image evaluation [19]. Recent studies have found that there is a lot of literature on the identification of parotid tumors with the help of radiomics, whether benign or malignant or PA and WT, but there is still a lack of standardized procedure analysis for parotid tumors [5,20-23].

Therefore, this study based on the radiomics features of MRI combined with clinical characteristics to establish a relevant prediction model, so as to better distinguish PA and WT, and offer improved support for clinical precision diagnosis and treatment.

Methods and materials

This is a retrospective study which was approved by the Ethics Committee of Shanghai Changzheng Hospital. The requirement for informed patient consent was waived due to the retrospective nature of the analysis and the anonymity of the data.

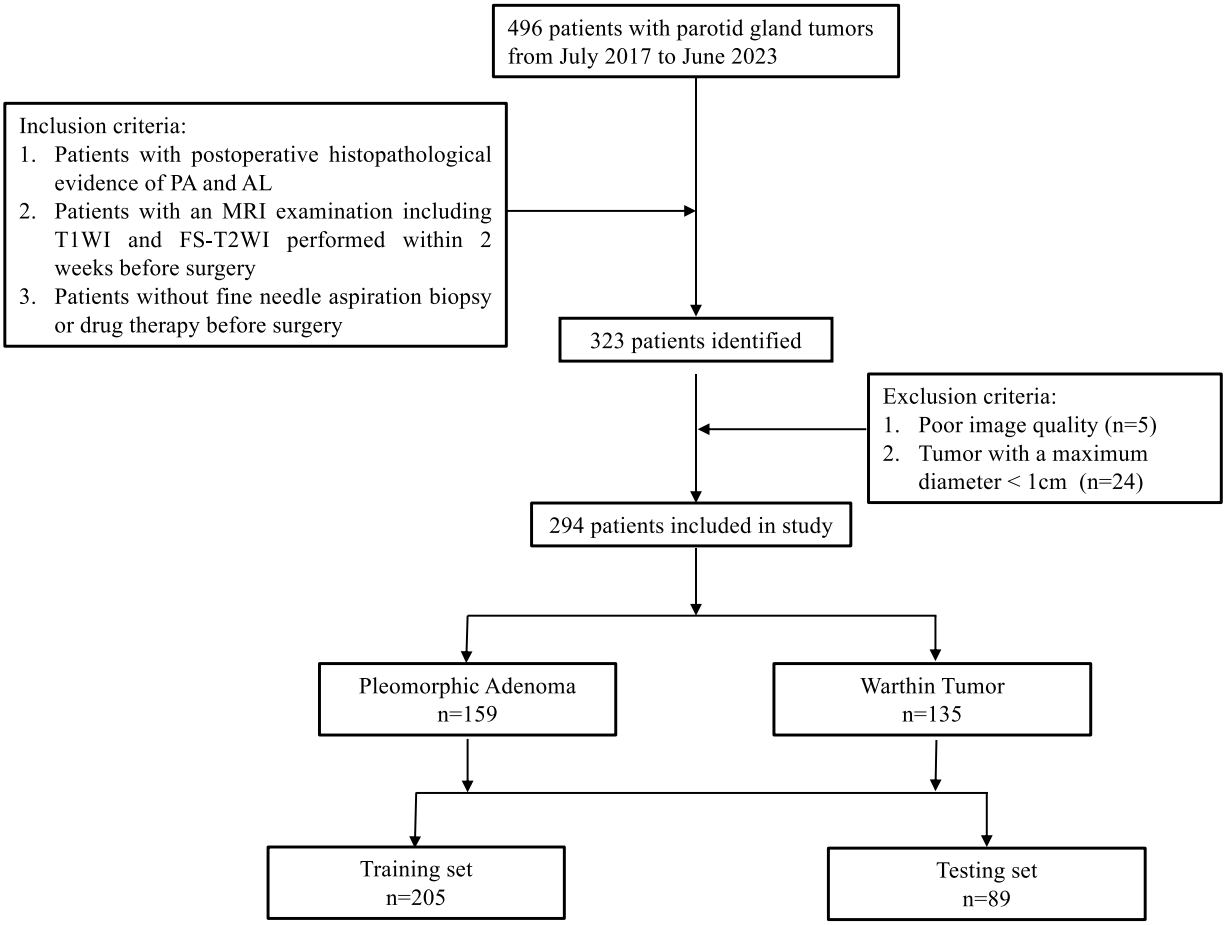

Fig. 1. The study flowchart used for case selection and the number of patients finally recruited per the inclusion and exclusion criteria.

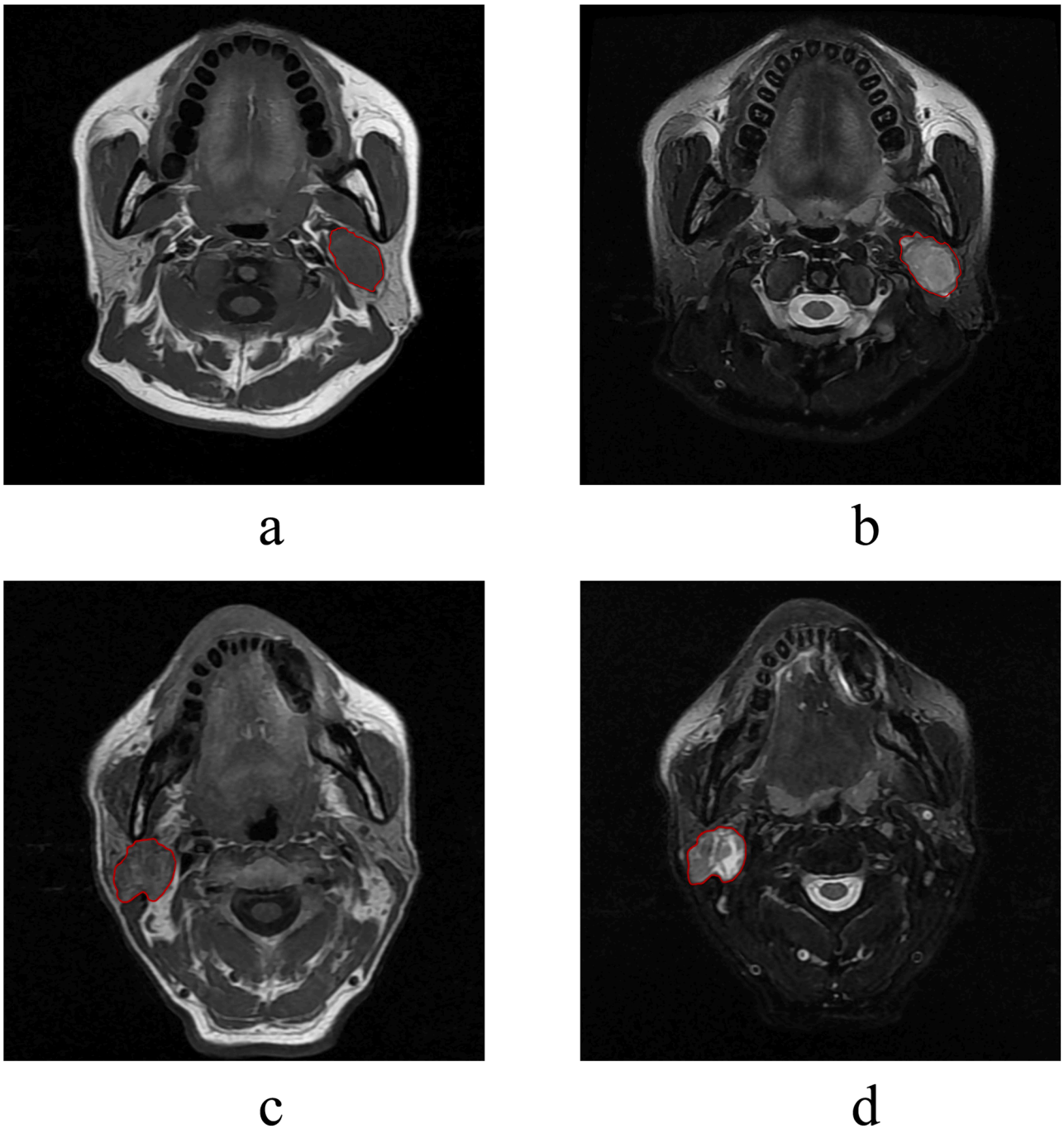

Fig. 2. Example of the manual segmentation of pleomorphic adenoma (2a&2b) and warthin tumor (2c&2d).

Patients

This study included patients with PA ($n = 159$) and WT ($n = 135$) confirmed by histopathology after parotid tumor surgery in our hospital from July 2017 to June 2023. The inclusion criteria were: 1) patients with postoperative histopathological evidence of PA and WT; 2) patients with an MRI examination including T1WI and FS-T2WI performed within 2 weeks before surgery; 3) patients without fine needle aspiration biopsy or drug therapy before examination. The exclusion criteria were: 1) Poor image quality; 2) Tumor with a maximum diameter < 1 cm [2, 8]. All patients were randomly divided into a training set and a testing set according to 7:3 [16,24]. Characteristics of patients and tumors are shown in Table 1. The research process is shown in Fig. 1.

MRI protocol

All patients underwent a 3.0T MRI scan (Philips Achieva 3.0T). The T1WI was acquired using the following parameters: echo time 8.5 ms; repetition time 550 ms; number of excitations 4; slice thickness 4 mm; slice spacing 1 mm; acquisition matrix 332 × 215; and field of view 259 × 199 cm. The parameters for the FS-T2WI sequence included: echo time 70 ms; repetition time 4226; number of excitations 2; slice thickness 4 mm; slice spacing 1 mm; acquisition matrix 260 × 182; field of view 230 × 230 cm.

Collection and evaluation of characteristics

Clinical factors, including sex, age, and smoking pack-years, were

Table 2
Univariate and multivariate logistic regression analysis of the predictive clinical factors in the training set.

Clinical	Univariate logistic regression analysis			Multivariate logistic regression analysis		
	p-value	OR	95 % CI	p-value	OR	95 %CI
Sex	<0.001	0.043	0.013–0.112	0.063	0.262	0.058–1.030
Age	<0.001	0.884	0.849–0.914	<0.001	0.859	0.794–0.915
Smoking	<0.001	0.856	0.819–0.889	<0.001	0.895	0.847–0.936
Shape	0.647	1.153	0.628–2.137			
Amount	<0.001	0.032	0.008–0.095	0.011	0.055	0.004–0.383
Margin	0.985	0.000	NA			

OR: odds ratio; CI: confidence interval.

collected. MRI radiological features were evaluated by two radiologists (H. S. and Q. C.) with 6 and 10 years of experience in head and neck radiology without knowing the histopathological results of tumors. Consensus was reached through discussion and negotiation in case of disagreement. The largest lesion was selected in patients with multiple tumors. The main MRI features evaluated are as follows: (a) Tumor shape (round/non-round); (b) Number of tumors (single/multiple); (c) Tumor margin (well or poorly defined).

MRI image outlining and segmentation

Two radiologists (H. S. and Q. C.) with 6 and 10 years of experience outlined the tumor on T1WI and FS-T2WI, slice by slice, using Radcloud software (v.7.7, Huiying Medical Technology Co., Ltd., China), focusing on the solid tumor components. Special care was taken to exclude cystic or necrotic areas, ensuring the ROIs reflected the tumor's solid pathology in Fig. 2. This meticulous process aimed to capture the tumor extent accurately while excluding non-tumor tissue. For cases with multiple lesions, the largest, most representative lesion was segmented, applying the same criteria to exclude cystic or necrotic changes.

3376 extracted features included four categories: (1) first-order features (to describe relatively intuitive geometric characteristics, such as the size, shape, surface roughness of lesions, etc.); (2) shape-based features (to describe relatively intuitive geometric properties); (3) texture features (to describe the spatial distribution information of ROI pixels, reflecting the spatial heterogeneity characteristics such as gray-scale changes, granularity, and roughness of the image); (4) wavelet transform-based features (Obtaining multi-resolution image description information by wavelet change of the original image).

MRI feature extraction and selection

30 randomly selected cases from the collected data were outlined independently by two radiologists to assess interobserver consistency [2,16]. Reader 1 outlined 30 cases again after a one-month interval. The inter-observer reliability and intra-observer repeatability of feature extraction were evaluated by using inter- and intra- class correlation (ICC), as ICC > 0.75 was considered reliable [7,25]. The remaining cases were outlined by Reader 1.

A large number of features extracted by Radcloud software may not be useful for a particular task. Dimensionality reduction and selection of task-specific features for best performance are necessary steps. To reduce redundant features and avoid overfitting, z-score normalization was applied as a preprocessing step. Pearson correlation coefficient was performed on the features consistent with normal distribution, otherwise, spearman's correlation analysis was performed. Finally, we used least absolute shrinkage and selection operator (LASSO) model, L1 regularization was used as the cost function, and the error value of cross validation is 5, and the maximum number of iterations is 1000, to identify and obtain the best radiomic features and develop radiomic models.

Construction of Rad-score and visualization of model

Using the linear combination of selected features, the Rad-score formula based on MRI image was generated, and the corresponding Rad-score was calculated. A combined model was constructed using logistic regression based on Rad-scores and clinical independent factors. Based on the performance of the three models, the best-performing model was selected to construct an intuitive radiomics nomogram, providing individualized predictions for the differentiation of PA and WT.

Statistical analysis

The statistical software used in this study was R software (version 4.3.1), and $P < 0.05$ was considered statistically significant. The Chi-square test is used to compare differences between qualitative variables and the Mann-Whitney U test was used to compare differences between quantitative variables.

Receiver operating characteristic (ROC) analysis was used to evaluate the clinical model, radiomics model and combined model in differentiating PA from WT. The efficacy of three models in the training set and testing set were evaluated t respectively by calculating the area under the curve (AUC) values and using Delong test. Decision curve analysis (DCA) was performed, based on quantitative calculation of the net benefits at a series of threshold probabilities, to evaluate the clinical utility of clinical model, radiomics model and combined model. Calibration curves were generated to analyze the fit degree and evaluate the consistency between the predicted results of radiomics nomogram and the actual state.

Results

Establishment of clinical model

Our study included 294 patients, and the clinical characteristics of all patients in the training and testing groups were summarized as shown in Table 1. In the training set and the testing set, there were significant differences in gender, age, smoking amount and tumor number. Univariate logistic regression analysis showed that gender, age, smoking amount, and number of tumors were significantly correlated with the identification of parotid PA and WT patients ($p < 0.001$). Multivariate logistic regression analysis showed that gender was significant on the margin ($p = 0.063$), while age ($p < 0.001$), smoking amount ($p < 0.001$), and number of tumors ($p = 0.011$) were still significant. Older age (OR, 0.884; 95 %CI, 0.849–0.914; $p < 0.001$), more smoking (OR, 0.856; 95 %CI, 0.819−0.889; $p < 0.001$), multiple lesions (OR, 0.032; 95 %CI, 0.008−0.095; $p < 0.001$) was more common in parotid WT patients. Age, amount of smoking, and number of tumors were identified as independent clinical risk factors in the clinical factor model in Table 2. The AUC of the clinical model was 0.966 in the training set and 0.954 in the testing set.

Table 3
Radiomics feature selection results.

Radiomics feature names	Coefficient
(Intercept)	0.40763664
T1WI: wavelet.LLH_ngtdm_Contrast	−0.5210558
T1WI: wavelet.HLL_gldm_LowGrayLevelEmphasis	−0.5075607
T1WI: wavelet.LHH_glszmLow_GrayLevelZoneEmphasis	−0.436313
T1WI: wavelet.LLL_glszm_SmallAreaLowGrayLevelEmphasis	−0.3870469
T1WI: wavelet.HHL_glszm_ZoneEntropy	−0.3245974
T1WI: wavelet.HHH_gldm_DependenceVariance	0.39504333
FS-T2WI: wavelet.LHL_firstorder_Kurtosis	−0.6188431
FS-T2WI: wavelet.HHL_gldm_LowGrayLevelEmphasis	−0.3470299
FS-T2WI: wavelet.HLL_glszm_ZoneEntropy	0.59756467
FS-T2WI: wavelet.LLH_glrlm_ShortRunHighGrayLevelEmphasis	0.76537243

Establishment of radiomics model

3168 stable radiomics features were selected from T1WI and FS-T2WI for subsequent dimension reduction analysis by ICC≥0.75. After applying Pearson's and Spearman's correlation analyses to eliminate highly correlated characteristics (with a threshold coefficient of |r| = 0.8), 556 feature values remained [20,26], and after lasso regression method, 42 feature values remained. Finally, 10 most prominent isagogic features were selected, the selected feature values are shown in Table 3. Fig. 3**a** shows the different hyperparameters (lambda values) associated with the diagnostic bias of different models. Fig. 3**b** describes the variation of LASSO coefficients of different texture parameters with hyperparameters. Use the following formula to determine the Rad-score: Rad-score = intercept + Σ (βi × Xi). Fig. 4 calculated Rad-score of PA (training set 2.650±1.350, testing set 2.121±1.400) was higher than that of WT (training set −2.380 ± 1.291, testing set −1.354±1.776),

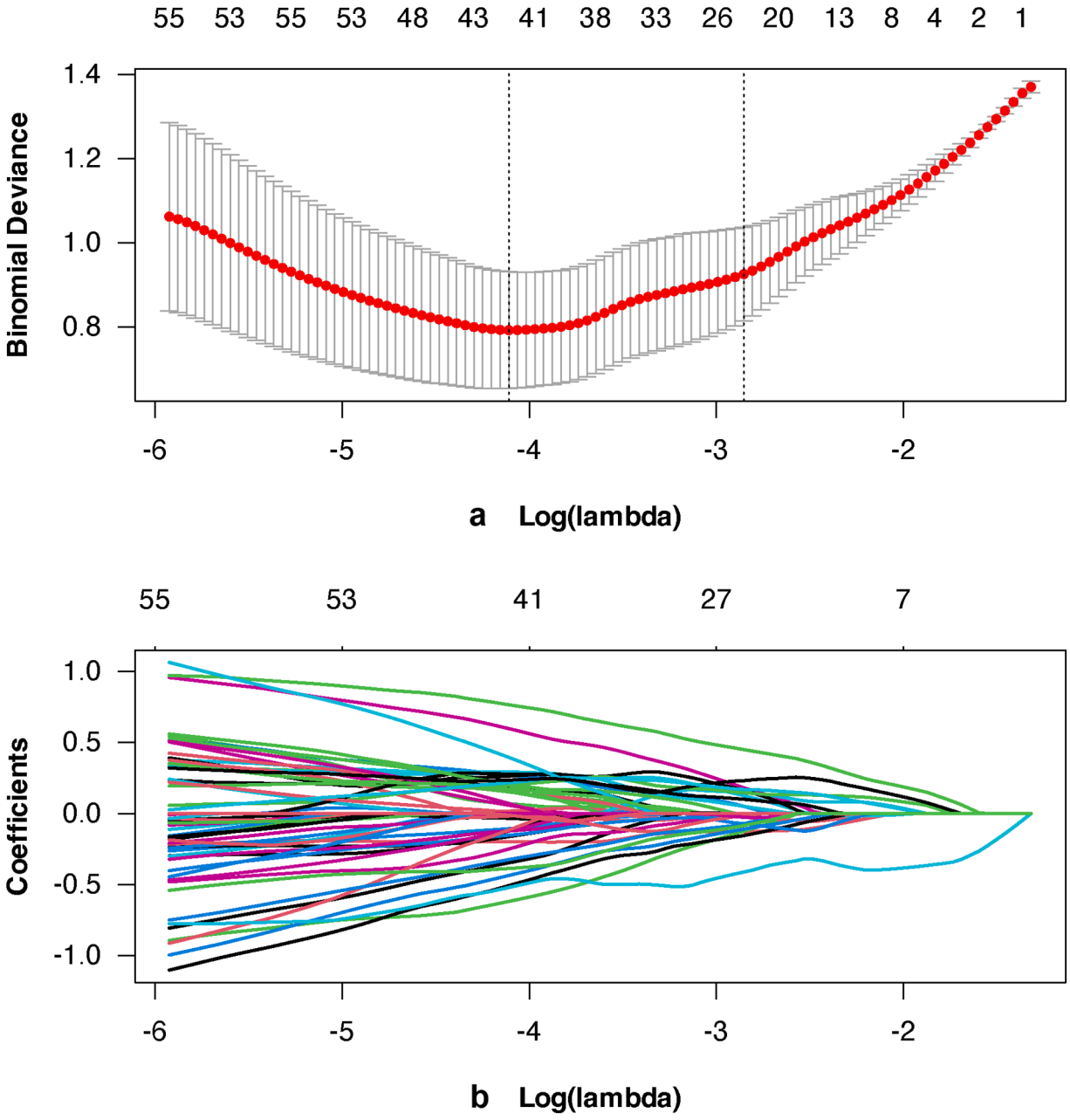

Fig. 3. Radiomics feature selection using the least absolute shrinkage and selection operator (LASSO) regression model. (3a) Different hyperparameters (lambda values) correspond to the deviations of different models. (3b) Change in different coefficients of LASSO with the hyperparameters (lambda values).

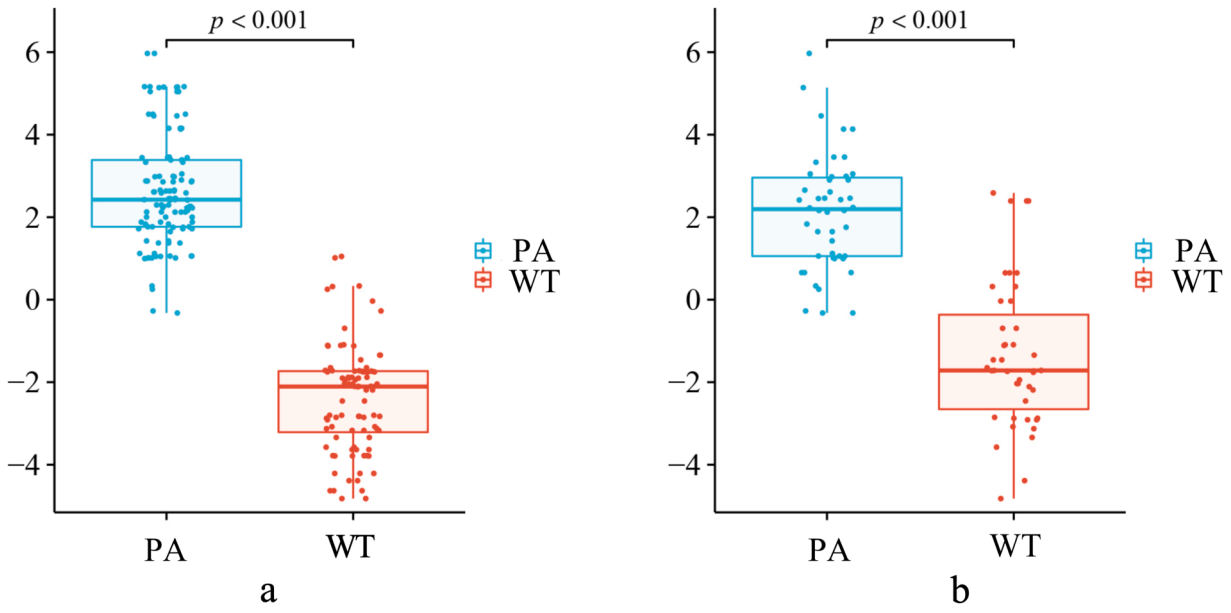

Fig. 4. The Rad-scores for each patient in the training (4a) and testing (4b) sets. Blue points represent the scores for PA patients, while red points represent the scores for WT patients.

Table 4
Performances of the three models in training and testing set.

Model	AUC	Accuracy	Precision	Recall	F-measure
Training set (n = 205)					
Clinical Model	0.966	0.932	0.923	0.956	0.939
Radiomics Model	0.952	0.863	0.883	0.867	0.875
Combined Model	0.998	0.971	0.973	0.973	0.973
Testing set (n = 89)					
Clinical Model	0.954	0.876	0.889	0.870	0.879
Radiomics Model	0.849	0.730	0.729	0.761	0.745
Combined Model	0.993	0.966	0.957	0.978	0.968

AUC: area under the curve.

which was statistically significant ($p < 0.001$).

Establishment of combined model and comparison between models

The combined model of training set was constructed by using Rad-scores and independent clinical factors, including age, smoking pack-years, and tumor amount. Performance of clinical model, radiomics model and combined model was shown in Table 4, including AUC values, accuracy, precision, recall and F-measure. ROC curves of the three models are shown in Fig. 5. Both clinical model and radiomics model obtained satisfactory prediction results, with AUC of 0.966 and 0.952 in the training set and 0.954 and 0.849 in the testing set, respectively. The combined model had the best prediction performance, and the AUC value was 0.998 on the training set and 0.993 on the testing set. Through DeLong test, each model is compared in pairs. Differences

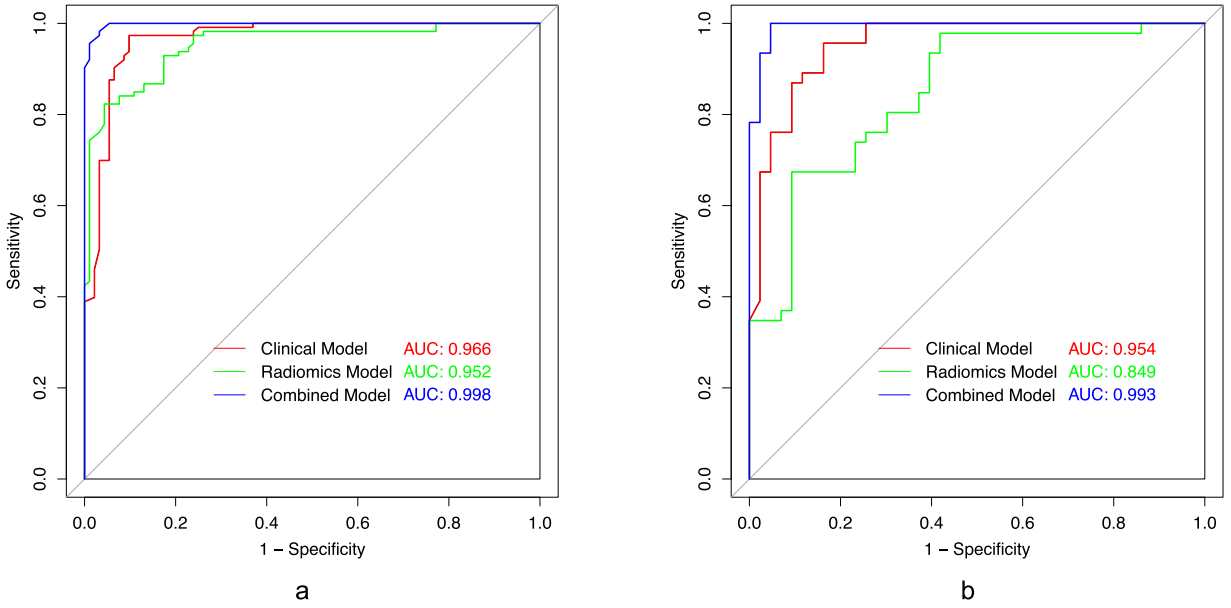

Fig. 5. The receiver operating characteristic (ROC) curves of the clinical model, the radiomics model, and the combined model in the training (5a) and testing (5b) sets, respectively.

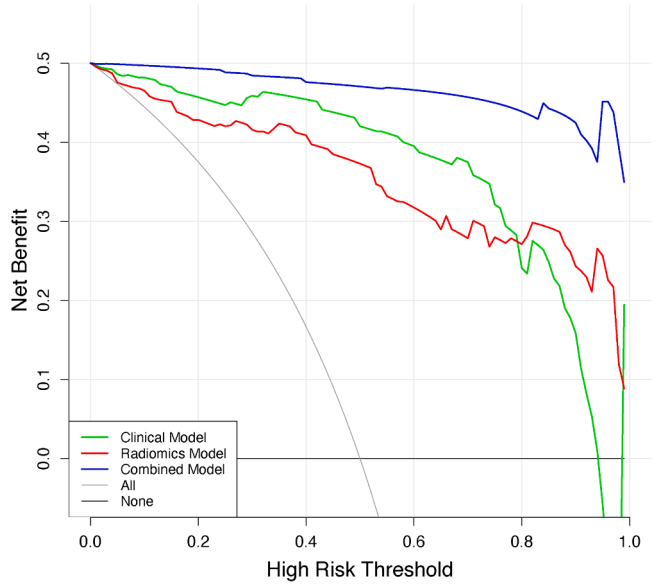

Fig. 6. Decision curve analysis for the three models. The y-axis indicatesthe net benefit, x-axis indicates threshold probability.

of training set clinical model vs. combined model, radiomics model vs. combined model; testing set clinical model vs radiomics model, clinical model vs combined model, radiomics model vs combined model were statistically significant ($p < 0.05$). Only difference between the training set clinical model and radiomics model was not statistically significant.

Establishment of radiomics nomogram

The DCA values of the three models are shown in Fig. 6, showing that over most threshold probability ranges, the combined model provides more overall net benefit in distinguishing parotid PA from WT than the radiomics model and the clinical model. The best-performing combined model was selected to construct an intuitive radiomics nomogram, providing individualized predictions for the differentiation of PA and WT, as presented in Fig. 7**a**. Calibration curves for the training set and testing set are shown in Fig. 7**b** and Fig. 7**c**, showing that the radiomics nomograms are well calibrated in both datasets.

Discussion

In this study, we developed and validated an intuitive radiomics nomogram based on clinical factors and MRI Rad-scores to distinguish PA from WT. The radiomics nomogram combined with independent clinical factors and Rad-scores based on T1WI and FS-T2WI performed best, with AUC of 0.998 and 0.993 for the training set and testing set, respectively, indicating that radiomics nomogram can distinguish PA from WT. It may provide a feasible and reliable non-invasive method for the evaluation of parotid tumors.

Between 2017–2021, five Head and Neck Surgery University Departments conducted multicenter prospective studies on 1929 patients in Poland [27]. In regions I-IV, around 90 % of tumors were benign, mainly PA and WT, while in region V, over 75 % were PA. Region V can saw a 40 % incidence of malignancy, notably in tumors larger than 4 cm or with facial nerve paresis. Despite benign appearances, imaging showed malignancy in 19 % of cases, but 38 % were false negatives for clinical and radiological signs of cancer.

Although both PA and WT are benign tumors, the biological behavior and treatment of PA and WT are different [28], meanwhile PA has a higher malignant tendency and a higher recurrence rate than WT [25]. This study underscores the need for heightened oncological vigilance and better preoperative preparation, given the clear visibility of parotid tumors [27].At present, Parotid fine needle aspiration is currently considered the gold-standard for diagnosis prior to surgical management [29], increasingly used for pathological analysis of parotid gland tumors [30]. However, as an invasive test, it may cause facial paralysis and the high incidence of inadequate diagnostic expectations is worrisome [31]. Therefore, it is very valuable to study the difference between PA and WT based on clinical information and radiological characteristics before biopsy.

Our study found that clinical information and radiomics features can be important factors in distinguishing PA from WT. In this study, we found that patients with WT were older and smoked more cigarettes than those with PA. Sex and amount of tumors showed significant differences between PA and WT. PA was mostly single tumor, and WT was not common in women. Our results are also consistent with previous findings. Feng et al. [25] found clear differences between PA and WT patients in age, sex, smoking history, and number of tumors. In our study, multivariate logistic regression analysis showed that age, smoking pack-years, and amount of tumor were independent predictors of PA and WT, which is consistent with previous studies. Zheng et al. [3] also considered shape of tumor as an independent clinical predictor in the PA vs. WT clinical model, which is inconsistent with our study.

Radiomics is a noninvasive method that performs quantitative analysis of features based on original images, builds models to obtain more information, and a priori identifies important diagnoses most likely to be contained within complex tumors in order to assess prognosis and guide individualized treatment [24,32,33]. Radiomics parameters such as contrast, zone entropy, low gray level emphasis, kurtosis, and dependence variance, extracted from T1WI and FS-T2WI sequences in this study, provide profound insights into the behavior of parotid gland PA and WT. These parameters reveal significant aspects of tumor heterogeneity, the presence of low-density areas, variations in tissue density and structure, and image complexity. They not only uncover the internal structural diversity and significant differences in tissue characteristics within tumors but also offer a new dimension by quantifying micro-variations, surpassing traditional qualitative imaging assessments. High values of zone entropy and contrast emphasize the complexity and potential malignant transformation of tumors, while parameters like low gray level emphasis and kurtosis help differentiate features between PA and WT, providing valuable information for clinical decision-making, optimizing patient treatment plans, and predicting tumor behavior. In summary, the integrated analysis of these radiomics parameters not only deepens our understanding of PA and WT behaviors but also paves new pathways for personalized patient management based on precision imaging.

Some previous studies combined radiomics features or Rad-scores [34-37] reported good predictive value in the differential diagnosis of parotid tumors. Gabelloni et al. [15] found that radiomic analysis of parotid tumors using T2-weighted MR Images was able to distinguish PA from WT with sensitivity, specificity, and diagnostic accuracy of 0.8695, 0.9062, and 0.8909, respectively. But they did not analyze clinical features that might be predictive. Hu et al. [22]. found that a radiomic-clinical model built by combining radiological features extracted from T2-weighted images with clinical factors helped distinguish PA from WT (training set 0.962, testing set 0.934). However, they did not include two important independent clinical risk predictors: smoking and the number of tumors. Based on this, our study selected 10 most important radiomics features from MRI T1WI and T2WI, included clinical predictors in the model, and quantified smoking in pack-years terms [38]. Our combined model obtained better AUC results (training set 0.998, testing set 0.993), which may also explain that the clinical model also obtained very good AUC results in distinguishing PA and WT (training set 0.966, testing set 0.954), which was better than radiomics model. Our results show that clinical predictors combined with radiomics extracted from MRI images can further improve the predictive performance of the model.

The study has some limitations. First, we lack DWI and dynamic

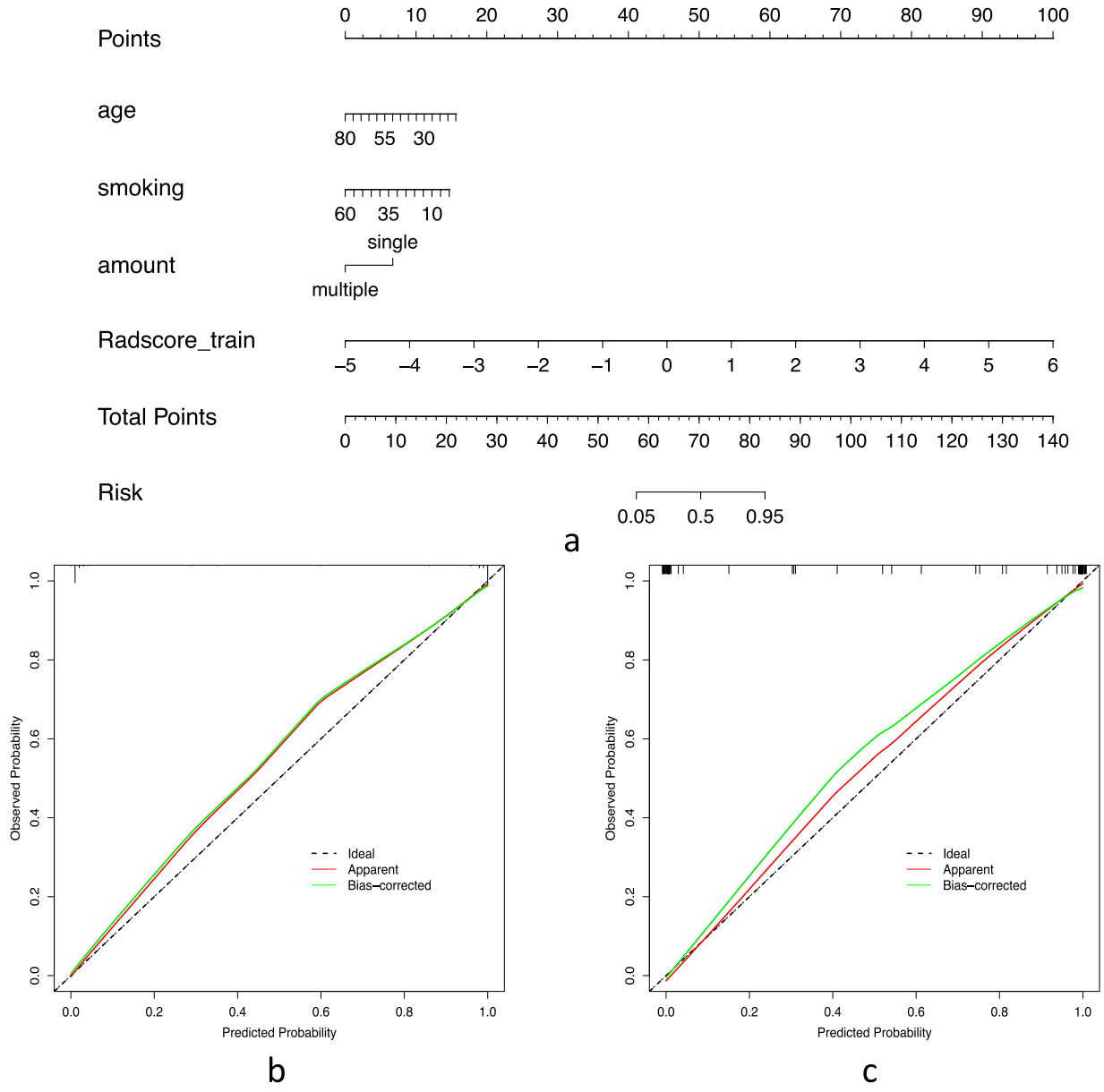

Fig. 7. (7a) The radiomics nomogram based on the training set, integrating age, smoking pack-years, amount of tumor, and Rad-scores. Risk means risk of the pleomorphic adenoma. Calibration curves of the radiomics nomogram in the training (7b) and testing (7c) sets. The 45° black line indicates the ideal prediction, the red line represents the predictive efficacy of the nomogram, and the green line represents the model performance trained after repeated self-sampling.

images, and these advanced sequences may continue to improve the performance of the model. Second, the data was collected in a single center, and no external validation data was used, limiting the robustness of our model to some extent. Again, our relatively small sample of patients overall and the different numbers of the two tumors could have prevented us from finding additional information or introduced bias due to the high number of one species. We look forward to multi-center and larger cohort studies and external validation to further confirm our conclusions in future. We will also add DWI and dynamic sequences in future work to explore whether these more advanced sequences can help improve model performance.

In conclusion, the establishment of an analytical model based on MRI radiomics can effectively classify benign parotid tumors, so this model can be used as an auxiliary diagnostic tool in clinical practice, especially for pre-surgical evaluation and decision-making. However, it should be noted that the radiomics nomogram can play an important complementary role at this stage, and still cannot replace the pathological diagnosis.

Ethics approval

This retrospective study was approved by the Ethics Committee of Shanghai Changzheng Hospital, all the patient information was anonymized, and informed consent forms were waived.

Data availability

The data are not publicly available due to privacy or ethical restrictions.

CRediT authorship contribution statement

Hongbiao Sun: Writing – review & editing, Writing – original draft, Methodology. **Zuoheng Sun:** Writing – original draft, Visualization, Data curation. **Wenwen Wang:** Writing – original draft, Methodology, Conceptualization. **Xudong Cha:** Software, Investigation. **Qinling Jiang:** Resources, Conceptualization. **Xiang Wang:** Methodology.

Qingchu Li: Formal analysis. **Shiyuan Liu:** Funding acquisition. **Huanhai Liu:** Software, Funding acquisition. **Qi Chen:** Writing – review & editing, Resources. **Weimin Yuan:** Writing – review & editing, Funding acquisition. **Yi Xiao:** Writing – review & editing, Writing – original draft, Project administration, Investigation, Funding acquisition.

Declaration of competing interest

The authors declare that they have no known competing financial interests or personal relationships that could have appeared to influence the work reported in this paper.

Funding

This study has received funding from the National Key Research and Development Program of China [No. 2022YFC2410000 & No. 2022YFC2410002]; the National Natural Science Foundation of China [No. 82271994]; the Military Commission Health Care Special Project [No. 22BJZ07]; the National Health Commission Capacity Building and Continuing Education Center [No. YXFSC2022JJSJ010]; the Shanghai Hospital Development Center [No. SHDC22022310-B]; Navy Medical University Teaching Achievement Cultivation Project [No. JPY2022B15]; Shanghai Changzheng Hospital Teaching Achievement Cultivation Project [No. JXPY2021B10].

References

[1] B. Wen, Z. Zhang, J. Zhu, L. Liu, Y. Li, H. Huang, et al., Apparent Diffusion Coefficient Map-Based Radiomics Features for Differential Diagnosis of Pleomorphic Adenomas and Warthin Tumors From Malignant Tumors, Front. Oncol. 12 (2022) 830496.
[2] Q. Yu, Y. Ning, A. Wang, S. Li, J. Gu, Q. Li, et al., Deep learning-assisted diagnosis of benign and malignant parotid tumors based on contrast-enhanced CT: a multicenter study, Eur. Radiol. 33 (9) (2023) 6054–6065.
[3] M. Zheng, Q. Chen, Y. Ge, L. Yang, Y. Tian, C. Liu, et al., Development and validation of CT-based radiomics nomogram for the classification of benign parotid gland tumors, Med. Phys. 50 (2) (2023) 947–957.
[4] Y. Mao, L.P. Jiang, J.L. Wang, F.Q. Chen, W.P. Zhang, Z.X. Liu, et al., Radiomic nomogram for discriminating parotid pleomorphic adenoma from parotid adenolymphoma based on grayscale ultrasonography, Front. Oncol. 13 (2024).
[5] Y. Lu, H. Liu, Q. Liu, S. Wang, Z. Zhu, J. Qiu, et al., CT-based radiomics with various classifiers for histological differentiation of parotid gland tumors, Front. Oncol. 13 (2023) 1118351.
[6] F. Chen, Y. Ge, S. Li, M. Liu, J. Wu, Y. Liu, Enhanced CT-based texture analysis and radiomics score for differentiation of pleomorphic adenoma, basal cell adenoma, and Warthin tumor of the parotid gland, Dentomaxillofac. Radiol. 52 (2) (2023) 20220009.
[7] Y.M. Zheng, J. Chen, Q. Xu, W.H. Zhao, X.F. Wang, M.G. Yuan, et al., Development and validation of an MRI-based radiomics nomogram for distinguishing Warthin's tumour from pleomorphic adenomas of the parotid gland, Dentomaxillofac. Radiol. 50 (7) (2021) 20210023.
[8] Y. Xu, Z. Shu, G. Song, Y. Liu, P. Pang, X. Wen, et al., The Role of Preoperative Computed Tomography Radiomics in Distinguishing Benign and Malignant Tumors of the Parotid Gland, Front. Oncol. 11 (2021) 634452.
[9] F.M. Hanege, O. Tuysuz, O. Sakallioglu, Arslan Solmaz O. Diagnostic value of preoperative fine needle aspiration cytology in parotid gland tumors, Diagn. Cytopathol. 48 (11) (2020) 1075–1080.
[10] Y.M. Zheng, J. Li, S. Liu, J.F. Cui, J.F. Zhan, J. Pang, et al., MRI-Based radiomics nomogram for differentiation of benign and malignant lesions of the parotid gland, Eur. Radiol. 31 (6) (2021) 4042–4052.
[11] L.L. Song, S.J. Chen, W. Chen, Z. Shi, X.D. Wang, L.N. Song, et al., Radiomic model for differentiating parotid pleomorphic adenoma from parotid adenolymphoma based on MRI images, BMC. Med. ImAging 21 (1) (2021) 54.
[12] Y.J. Jung, M. Han, E.J. Ha, J.W. Choi, Differentiation of salivary gland tumors through tumor heterogeneity: a comparison between pleomorphic adenoma and Warthin tumor using CT texture analysis, Neuroradiology. 62 (11) (2020) 1451–1458.
[13] T. Yamamoto, H. Kimura, K. Hayashi, Y. Imamura, M. Mori, Pseudo-continuous arterial spin labeling MR images in Warthin tumors and pleomorphic adenomas of the parotid gland: qualitative and quantitative analyses and their correlation with histopathologic and DWI and dynamic contrast enhanced MRI findings, Neuroradiology. 60 (8) (2018) 803–812.
[14] F. Piludu, S. Marzi, M. Ravanelli, R. Pellini, R. Covello, I. Terrenato, et al., MRI-Based Radiomics to Differentiate between Benign and Malignant Parotid Tumors With External Validation, Front. Oncol. 11 (2021) 656918.
[15] M. Gabelloni, L. Faggioni, S. Attanasio, V. Vani, A. Goddi, S. Colantonio, et al., Can Magnetic Resonance Radiomics Analysis Discriminate Parotid Gland Tumors? A Pilot Study. Diagnos. (Basel). 10 (11) (2020).
[16] Y.M. Zheng, W.J. Xu, D.P. Hao, X.J. Liu, C.P. Gao, G.Z. Tang, et al., A CT-based radiomics nomogram for differentiation of lympho-associated benign and malignant lesions of the parotid gland, Eur. Radiol. 31 (5) (2021) 2886–2895.
[17] Y. Liu, H. Shi, S. Huang, X. Chen, H. Zhou, H. Chang, et al., Early prediction of acute xerostomia during radiation therapy for nasopharyngeal cancer based on delta radiomics from CT images, Quant. ImAging Med. Surg. 9 (7) (2019) 1288–1302.
[18] M.H. Zhang, A. Hasse, T. Carroll, A.T. Pearson, N.A. Cipriani, D.T. Ginat, Differentiating low and high grade mucoepidermoid carcinoma of the salivary glands using CT radiomics, Gland. Surg. 10 (5) (2021) 1646–1654.
[19] Y. Liu, J. Zheng, X. Lu, Y. Wang, F. Meng, J. Zhao, et al., Radiomics-based comparison of MRI and CT for differentiating pleomorphic adenomas and Warthin tumors of the parotid gland: a retrospective study, Oral Surg. Oral Med. Oral Pathol. Oral Radiol. 131 (5) (2021) 591–599.
[20] J. Qi, A. Gao, X. Ma, Y. Song, G. Zhao, J. Bai, et al., Differentiation of Benign From Malignant Parotid Gland Tumors Using Conventional MRI Based on Radiomics Nomogram, Front. Oncol. 12 (2022) 937050.
[21] K. Mao, L.M. Wong, R. Zhang, T.Y. So, Z. Shan, K.F. Hung, et al., Radiomics Analysis in Characterization of Salivary Gland Tumors on MRI: a Systematic Review, Cancers. (Basel) 15 (20) (2023).
[22] Z. Hu, J. Guo, J. Feng, Y. Huang, H. Xu, Q. Zhou, Value of T2-weighted-based radiomics model in distinguishing Warthin tumor from pleomorphic adenoma of the parotid, Eur. Radiol. 33 (6) (2023) 4453–4463.
[23] Z.F. Xu, Y.B. Jin, W.X. Wu, J.M. Wu, B. Luo, C.L. Zeng, et al., Machine learning-based multiparametric traditional multislice computed tomography radiomics for improving the discrimination of parotid neoplasms, Mol. Clin. Oncol. 15 (5) (2021).
[24] Y. Zheng, D. Zhou, H. Liu, M. Wen, CT-based radiomics analysis of different machine learning models for differentiating benign and malignant parotid tumors, Eur. Radiol. 32 (10) (2022) 6953–6964.
[25] B. Feng, Z. Wang, J. Cui, J. Li, H. Xu, D. Yu, et al., Distinguishing parotid polymorphic adenoma and Warthin tumor based on the ct radiomics nomogram: a multicenter study, Acad. Radiol. 30 (4) (2023) 717–726.
[26] Y. He, B. Hu, C. Zhu, W. Xu, Y. Ge, X. Hao, et al., A novel multimodal radiomics model for predicting prognosis of resected hepatocellular carcinoma, Front. Oncol. 12 (2022) 745258.
[27] M. Wierzbicka, E. Bartkowiak, W. Pietruszewska, D. Stodulski, J. Markowski, P. Burduk, et al., Rationale for increasing oncological vigilance in relation to clinical findings in accessory parotid gland-observations based on 2192 cases of the polish salivary network database, Cancers. (Basel) 16 (2) (2024).
[28] M. Quer, J.C. Hernandez-Prera, C.E. Silver, M. Casasayas, R. Simo, V. Vander Poorten, et al., Current trends and controversies in the management of Warthin tumor of the parotid gland, Diagnostics. (Basel) 11 (8) (2021).
[29] F. Vernuccio, F. Arnone, R. Cannella, B. Verro, A. Comelli, F. Agnello, et al., Diagnostic performance of qualitative and radiomics approach to parotid gland tumors: which is the added benefit of texture analysis? Br. J. Radiol. 94 (1128) (2021).
[30] M. Suzuki, R. Kawata, M. Higashino, S. Nishikawa, T. Terada, S.I. Haginomori, et al., Values of fine-needle aspiration cytology of parotid gland tumors: a review of 996 cases at a single institution, Head Neck 41 (2) (2019) 358–365.
[31] Y.Y. Xu, Z.Y. Shu, G. Song, Y.J. Liu, P.P. Pang, X.H. Wen, et al., The role of preoperative computed tomography radiomics in distinguishing benign and malignant tumors of the parotid gland, Front. Oncol. (2021) 11.
[32] R.J. Gillies, P.E. Kinahan, H. Hricak, Radiomics: images are more than pictures, they are data, Radiology. 278 (2) (2016) 563–577.
[33] L. Faggioni, M. Gabelloni, F. De Vietro, J. Frey, V. Mendola, D. Cavallero, et al., Usefulness of MRI-based radiomic features for distinguishing Warthin tumor from pleomorphic adenoma: performance assessment using T2-weighted and post-contrast T1-weighted MR images, Eur. J Radiol. Open 9 (2022).
[34] Z. He, Y. Mao, S. Lu, L. Tan, J. Xiao, P. Tan, et al., Machine learning–based radiomics for histological classification of parotid tumors using morphological MRI: a comparative study, Eur. Radiol. 32 (12) (2022) 8099–8110.
[35] D.D. Muntean, S.M. Dudea, M. Băciuț, C. Dinu, S. Stoia, C. Solomon, et al., The role of an MRI-based radiomic signature in predicting malignancy of parotid gland tumors, Cancers. (Basel) 15 (13) (2023) 3319.
[36] Y-m Zheng, J. Li, S. Liu, J-f Cui, J-f Zhan, J. Pang, et al., MRI-Based radiomics nomogram for differentiation of benign and malignant lesions of the parotid gland, Eur. Radiol. 31 (6) (2021) 4042–4052.
[37] D.D. Muntean, L.M. Lenghel, P.A. Ștefan, D. Fodor, M. Bădărînză, C. Csutak, et al., Radiomic features associated with lymphoma development in the parotid glands of patients with primary Sjögren’s syndrome, Cancers. (Basel) 15 (5) (2023) 1380.
[38] A.H. Krist, K.W. Davidson, C.M. Mangione, M.J. Barry, M. Cabana, A.B. Caughey, et al., Screening for lung cancer: US preventive services task force recommendation statement, JAMa 325 (10) (2021) 962–970.